DOI: 10.1002/chem.200701778

Copper(II) Coordination Chemistry of Westiellamide and Its Imidazole, Oxazole, and Thiazole Analogues

Peter Comba,*[a] Lawrence R. Gahan,[b] Gebhard Haberhauer,[c] Graeme R. Hanson,[d] Christopher J. Noble,[d] Björn Seibold,[a] and Anna L. van den Brenk[b]

Abstract: The copper(II) coordination chemistry of westiellamide (H_3L^{wa}), as well as of three synthetic analogues with an [18]azacrown-6 macrocyclic structure but with three imidazole (H_3L^1), oxazole (H_3L^2), and thiazole (H_3L^3) rings instead of oxazoline, is reported. As in the larger patellamide rings, the $N_{heterocycle}$-$N_{peptide}$-$N_{heterocycle}$ binding site is highly preorganized for copper(II) coordination. In contrast to earlier reports, the macrocyclic peptides have been found to form stable mono- and dinuclear copper(II) complexes. The coordination of copper(II) has been monitored by high-resolution electrospray mass spectrometry (ESI-MS), spectrophotometric and polarimetric titrations, and EPR and IR spectroscopies, and the structural assignments have been supported by time-dependent studies (UV/Vis/NIR, ESI-MS, and EPR) of the complexation reaction of copper(II) with H_3L^1. Density functional theory (DFT) calculations have been used to model the structures of the copper(II) complexes on the basis of their spectroscopic data. The copper(II) ion has a distorted square-pyramidal geometry with one or two coordinated solvent molecules (CH_3OH) in the mononuclear copper(II) cyclic peptide complexes, but the coordination sphere in $[Cu(H_2L^{wa})(OHCH_3)]^+$ differs from those in the synthetic analogues, $[Cu(H_2L)(OHCH_3)_2]^+$ (L = L^1, L^2, L^3). Dinuclear copper(II) complexes ($[Cu^{II}_2(HL)(\mu\text{-}X)]^+$; X = OCH_3, OH; L = L^1, L^2, L^3, L^{wa}) are observed in the mass spectra. While a dipole–dipole coupled EPR spectrum is observed for the dinuclear copper(II) complex of H_3L^3, the corresponding complexes with H_3L (L = L^1, L^2, L^{wa}) are EPR-silent. This may be explained in terms of strong antiferromagnetic coupling (H_3L^1) and/or a low concentration of the dicopper(II) complexes (H_3L^{wa}, H_3L^2), in agreement with the mass spectrometric observations.

Keywords: coordination modes · copper · crown compounds · macrocycles · peptides

Introduction

Small macrocyclic peptides isolated from the ascidian *Lissoclinum patella* and *bistratum* have attracted significant attention over the last twenty years, but the biological function of these macrocycles in the ascidian metabolism is still uncertain.[1–19] The geometric arrangement of the functional groups and the size of the macrocycles suggest that their

[a] Prof. Dr. P. Comba, B. Seibold
Universität Heidelberg, Anorganisch-Chemisches Institut
Im Neuenheimer Feld 270, 69120 Heidelberg (Germany)
Fax: (+49) 6221-546617
E-mail: peter.comba@aci.uni-heidelberg.de

[b] Prof. Dr. L. R. Gahan, Dr. A. L. van den Brenk
The University of Queensland
School of Molecular and Microbial Sciences
Brisbane, Queensland 4072 (Australia)

[c] Prof. Dr. G. Haberhauer
Institut für Organische Chemie, Universität Duisburg-Essen
Universitätsstraße 5, 45177 Essen (Germany)

[d] Prof. Dr. G. R. Hanson, Dr. C. J. Noble
The University of Queensland, Centre for Magnetic Resonance
Brisbane, Queensland 4072 (Australia)

Supporting information for this article is available on the WWW under http://www.chemeurj.org/ or from the author: Table S1: A detailed list of the observed exact masses (electrospray mass spectrometry). Table S2: g- and A-strain linewidth (10^{-4} cm^{-1}) parameters for the mononuclear copper(II) complexes $[Cu^{II}(H_2L)]^+$, (L = L^1, L^2, L^3, L^{wa}) (X-band EPR spectroscopy). Table S3: A detailed list of distances and angles of structures a)–h) (Figure 8). Figure S1: X-band EPR spectra (130 K) of mixtures of copper(II) triflate, ($n$$Bu_4N$)(OMe), and H_3L^1 in methanol [copper(II)/base/ligand]. Figure S2: Expansion of the experimental and simulated second-derivative X-band EPR spectra between 310 and 340 mT of the mononuclear copper(II) complexes ($[Cu^{II}(H_2L)]^+$ (L = L^1, L^2, L^3, L^{wa})) in methanol at 50 K (Figure 4)

biological purpose is to bind metal ions. The function of the corresponding complexes may be metal ion transport or catalysis. Some cyclic peptides have been found to display cytotoxic, antibacterial, or antiviral activity.[20–26] There have been examples of cyclic peptides being active in cases of multi-drug resistance or serving as antineoplastic agents.[27,28] The abilities of ascidiacyclamide, patellamides, and some synthetic analogues to bind copper(II) ions with high specificity in their 24-membered azacrown-8 macrocycles have been thoroughly studied.[5,6,8,12,14–16,18,19,29] Herein, we describe the copper(II) coordination chemistry of the smaller 18-membered azacrown-6 macrocycle westiellamide (H_3L^{wa}) as well as of three synthetic analogues, H_3L^1, H_3L^2, and H_3L^3 (see below). Westiellamide (H_3L^{wa}) was isolated from

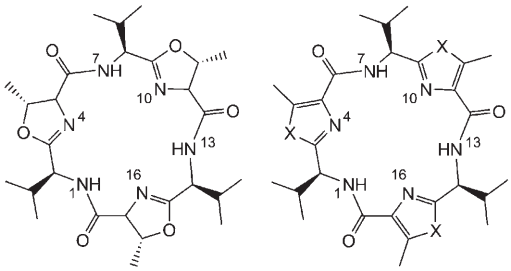

the ascidian *Lissoclinum bistratum*, although its synthesis has also been reported.[30–32] The macrocycles H_3L ($L = L^{wa}$, L^1, L^2, L^3) have a common backbone, derived from L-valine amino acid residues, and differ only in their oxazoline, oxazole, imidazole, and thiazole heterocyclic donor groups. The synthesis and characterization of the derivatives H_3L^1, H_3L^2, and H_3L^3 have been described previously.[33,34]

Compounds H_3L^{wa} and H_3L^1, H_3L^2, and H_3L^3 have an alternating sequence of heterocyclic nitrogen lone pairs and peptide nitrogen donors in a highly preorganized arrangement. NMR studies have indicated that the conformations in the solid state and in solution are identical.[31,35] An overlay plot of the crystallographically determined structures of H_3L^{wa} and H_3L^1 shows the similarity of these two ligands with respect to the shape and size of the macrocyclic cavity, although there are significant differences in the conformations (Figure 1).[32,33] With the constant $N_{heterocycle}$-$N_{peptide}$-$N_{heterocycle}$ binding site and strongly different nucleophilicities of the heterocyclic nitrogen donors (pK_a(*N*-methylimidazole) = 7.0, pK_a(oxazole) = 0.8, pK_a(thiazole) = 2.5), we present a set of three ligands which allows us to structurally model the naturally occurring cyclic peptide westiellamide H_3L^{wa} (pK_a(oxazoline) = 4.8).

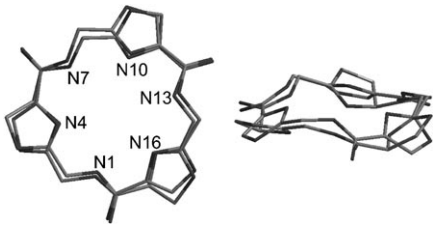

Figure 1. Overlay plot of the X-ray crystal structural data of H_3L^{wa} and H_3L^1. Average distances [Å] ($\Delta_{max} = \pm 0.06$ Å) of the same type of nitrogen donor atoms ($N_{hetcycl}$-$N_{hetcycl}$/N_{amide}-N_{amide}): L^{wa} (4.25/4.70), L^1 (4.39/5.08), L^2 (4.27/5.12), L^3 (4.55/4.97).[32,33]

Systematic metal-ion-binding studies with westiellamide have revealed an affinity for silver(I) involving the formation of a cluster with four silver(I) ions sandwiched by two H_3L^{wa} macrocycles.[1,36] It was concluded that other metal ions, including copper(II), are not coordinated by the macrocyclic ligand and interact only weakly with westiellamide. We now report the formation of stable mononuclear copper(II) complexes with the naturally occurring H_3L^{wa} and the artificial macrocycles H_3L^1, H_3L^2, and H_3L^3. More importantly, with westiellamide H_3L^{wa} and the three artificial structural analogues H_3L^1, H_3L^2, and H_3L^3, we have also obtained spectroscopic evidence and have been able to compute stable structures for dinuclear copper(II) complexes bridged by a methoxide or hydroxide anion. The formation of the mono- and dinuclear complexes involves a metal-ion-assisted deprotonation of an amide nitrogen donor. Structures and solution properties of the copper(II) complexes of H_3L^{wa} and H_3L^1, H_3L^2, and H_3L^3 are discussed on the basis of spectroscopic data (ESI-MS, UV/Vis/NIR, EPR), spectra simulations, spectrophotometric and polarimetric titrations, and DFT-based model calculations. These complexes are notoriously difficult to isolate as pure materials and they are difficult to crystallize. One of the dinuclear complexes, $[Cu^{II}_2(HL^1)(\mu\text{-}OCH_3)](CF_3SO_3)$, has been isolated and characterized, and its spectroscopic and magnetic data have confirmed the conclusions based on the solution spectra and computational data.

Results and Discussion

Mass spectrometry: High-resolution ESI mass spectrometry was used to identify charged complexes in solutions of the macrocycles, copper(II) trifluoromethanesulfonate (triflate), and base [(nBu$_4$N)(OMe) or NEt$_3$] in various solvents (details of the experimental and calculated exact masses are given as Supporting Information, Table S1). The relevant copper(II) species were monopositive complex cations throughout, and no negatively charged complexes were detected. It soon became apparent that with one copper(II) ion coordinated, the macrocycles are deprotonated at one (amide) site, whereas with two copper(II) ions coordinated, three sites are deprotonated (three amides, or two amides and one aqua or methanol ligand, producing bridging hydroxide or methoxide anions). Spectra featuring signals for the protonated metal-free macrocycles at m/z 547.3 $[H_4L^{wa}]^+$, 580.4 $[H_4L^1]^+$, 541.3 $[H_4L^2]^+$, and 589.2 $[H_4L^3]^+$, together with those of the mononuclear complexes at m/z 608.2 $[Cu^{II}(H_2L^{wa})]^+$, 641.3 $[Cu^{II}(H_2L^1)]^+$, 602.2 $[Cu^{II}(H_2L^2)]^+$, and 650.1 $[Cu^{II}(H_2L^3)]^+$, were obtained from solutions of copper(II) and the macrocycles without the addition of base.

This indicates that deprotonation of one of the amide groups ($pK_a \approx 15$) is assisted by copper(II), and that these protons are captured by the metal-free macrocycles.[37]

In absolutely dry aprotic solvents, such as acetonitrile, only the mononuclear $[Cu^{II}(H_2L)]^+$ complexes ($L = L^{wa}$, L^1, L^2, L^3) were observed. However, in the presence of traces of water in acetonitrile (water content: 0.001 %) peaks for the putative μ-OH-bridged dinuclear species at *m*/*z* 720.2 $[Cu^{II}_2(HL^1)(\mu\text{-}OH)]^+$ and 729.1 $[Cu^{II}_2(HL^3)(\mu\text{-}OH)]^+$ could also be detected. In the presence of methanol, signals of the dinuclear methoxide-bridged complexes at *m*/*z* 701.2 $[Cu^{II}_2(HL^{wa})(\mu\text{-}OCH_3)]^+$, 734.2 $[Cu^{II}_2(HL^1)(\mu\text{-}OCH_3)]^+$, 695.1 $[Cu^{II}_2(HL^2)(\mu\text{-}OCH_3)]^+$, and 743.1 $[Cu^{II}_2(HL^3)(\mu\text{-}OCH_3)]^+$ were observed, in addition to the signals of the mononuclear species. No μ-OH-bridged dinuclear copper(II) complexes were observed in methanol. Exact masses and isotope distributions, together with the calculated spectra for the mono- and dinuclear copper(II) complexes with H_3L^1 and H_3L^{wa}, are shown in Figure 2.

The relative intensities of the *m*/*z* peaks of the mono- and dinuclear complexes in methanol are strongly dependent on the concentration of base. With an excess of base, the peaks for the mononuclear complex $[Cu^{II}(H_2L^1)]^+$ and the corresponding metal-free macrocycle $[H_4L^1]^+$ vanish at the expense of those of the dinuclear complex $[Cu^{II}_2(HL^1)(\mu\text{-}OCH_3)]^+$. However, the mononuclear complex $[Cu^{II}(H_2L^3)]^+$ is not completely transformed to the dinuclear $[Cu^{II}_2(HL^3)(\mu\text{-}OCH_3)]^+$ and metal-free ligand, and, with the macrocycles H_3L^{wa} and H_3L^2, only weak signals for $[Cu^{II}_2(HL)(\mu\text{-}OCH_3)]^+$ are detected at variable ligand/base/copper(II) concentration ratios. The preference for the formation of the dicopper(II) complex with the imidazole-based ligand L^1 suggests that the coordination of the first copper(II) center preorganizes the second coordination site. This cooperativity may be further assisted by coordinated methanol donors, which may act as anchors for the second copper(II) ion. The differences in the relative stabilities (mono- vs dinuclear) of the complexes with the four macrocyclic ligands can thus be attributed to a combination of various effects, that is, the nucleophilicities of the heterocyclic donors ($pK_a(H_3L^3, H_3L^2, H_3L^1, H_3L^{wa})$ ~2.5 vs. ~0.8 vs. ~7.0 vs. ~4.8) and structural differences in the macrocycles due to the electronic structures of the amide-substituted heterocycles (see also Figure 1).[31,35]

Spectrophotometric and polarimetric titrations: The above interpretation of the mass spectrometric data was fully supported by the results of spectrophotometric titrations of solutions of the macrocycle H_3L^1 and copper(II) triflate with base (NEt_3 in acetonitrile or $(n\text{Bu}_4\text{N})(OCH_3)$ in methanol) at constant ionic strength [$\mu = 0.1$ M, $(n\text{Bu}_4\text{N})(ClO_4)$]; the titration experiments with H_3L^1 are presented here as an example. In agreement with the predicted deprotonation of one or two (three) peptide amide groups upon complexation of H_3L^1 to one or two copper(II) ions, the UV/Vis spectra (Figure 3a, b) reveal end-points after the addition of one or three equivalents of base, respectively (insets in Figure 3a, b). The UV/Vis/NIR spectra of a titration of a 1:1 mixture of H_3L^1 and copper(II) triflate in acetonitrile with NEt_3 are shown in Figure 3a. The absorption reaches an inflection point after the addition of approximately one equivalent of base (inset in Figure 3a). The d–d transition at 716 nm ($\varepsilon \approx 110\ M^{-1}cm^{-1}$) and a charge-transfer transition at 360 nm ($\varepsilon \approx 600\ M^{-1}cm^{-1}$) in acetonitrile are assigned to the chromophore of the $[Cu^{II}(H_2L^1)(NCCH_3)_n]^+$ complex. The consumption of only one equivalent of base indicates that the copper(II) ion is coordinated to an $N_{heterocycle}$-$N_{peptide}$-$N_{heterocycle}$ motif. The overall absorption increases again after

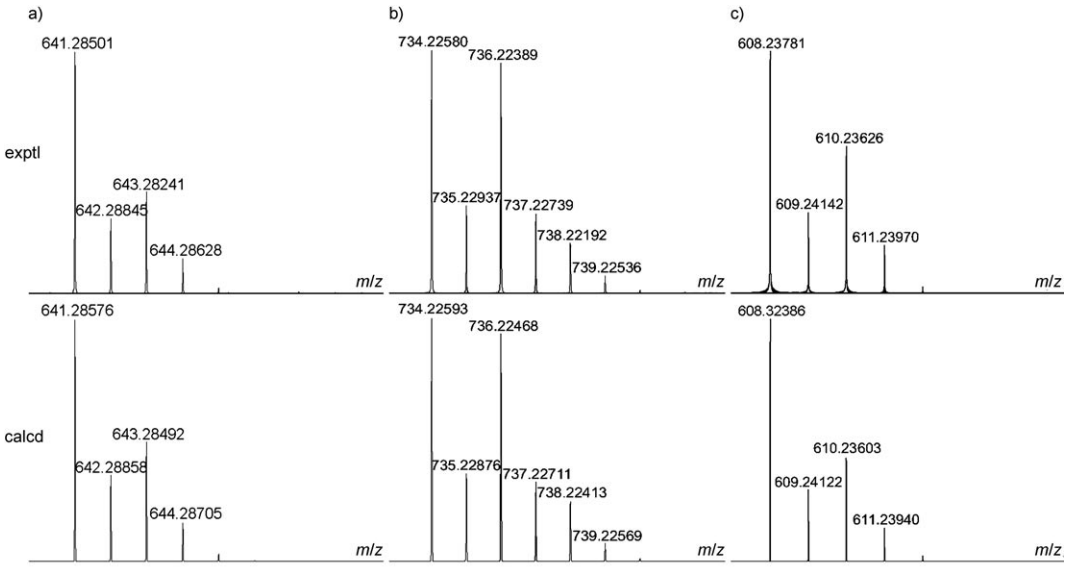

Figure 2. Experimental and calculated isotope distributions of the mono- and dinuclear copper(II) complexes of a) $[Cu^{II}(H_2L^1)]^+$, b) $[Cu^{II}_2(HL^1)(\mu\text{-}OCH_3)]^+$, c) $[Cu^{II}(H_2L^{wa})]^+$.

the inflection point. ESI mass spectra of these mixtures reveal the hydroxo-bridged dinuclear $[Cu^{II}_2(HL^1)(NCCH_3)_n(\mu\text{-}OH)]^+$ complex described above (note that throughout we do not specify the number of coordinated solvent molecules; in the ESI-MS experiments $n=0$, in solution n is generally 2 for the dinuclear complexes, that is, one terminal solvent molecule per copper(II) center, and $n=1$ or 2 for the mononuclear copper(II) complexes).

The spectrophotometric titration of a 1:2 mixture of H_3L^1 and copper(II) triflate with methoxide is shown in Figure 3b. The addition of base is accompanied by a change of color of the solution from yellow to blue. Addition of excess base leads to the precipitation of a blue solid. The absorption reaches a maximum after the addition of three equivalents of base, consistent with the formation of $[Cu^{II}_2(HL^1)(\mu\text{-}OCH_3)(OHCH_3)_n]^+$, again in agreement with the ESI-MS results. Similar behavior is observed with NEt_3 as the base in methanol. All spectra show strong ligand-to-metal charge-transfer (LMCT) transitions in the UV region. The d-d transitions at 716 nm ($\varepsilon \approx 90\,M^{-1}cm^{-1}$) and 565 nm ($\varepsilon \approx 55\,M^{-1}cm^{-1}$, shoulder), which appear after the addition of three equivalents of base, are assigned to the dinuclear complex $[Cu^{II}_2(HL^1)(\mu\text{-}OCH_3)(OHCH_3)_n]^+$. A comparison of the results of the titrations in methanol and acetonitrile supports the interpretation derived from the ESI-MS experiments that a bridging ligand (methoxide or hydroxide) is required for the formation of the dicopper(II) compounds.

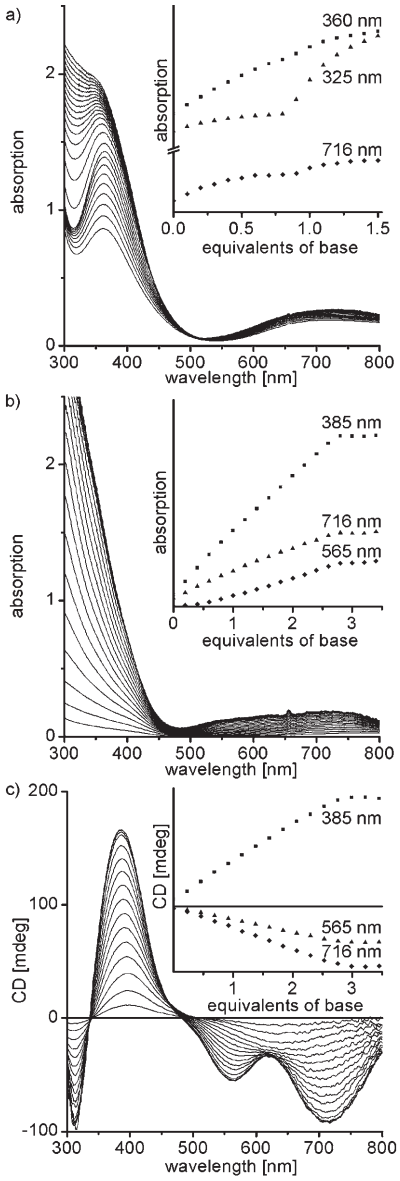

Figure 3. a) Titration of H_3L^1/Cu^{2+} with NEt_3 in acetonitrile ($c(H_3L^1)=2$ mM); b) titration of H_3L^1/Cu^{2+} with CH_3O^- in methanol ($c(H_3L^1)=2$ mM); c) titration of H_3L^1/Cu^{2+} with NEt_3 in methanol ($c(H_3L^1)=2$ mM).

Titration of a 1:2 mixture of H_3L^1 and copper(II) triflate with NEt_3, monitored by CD spectroscopy, confirmed the formation of chiral copper(II) complexes upon addition of base (Figure 3c). Initially, an increase of a negative Cotton effect at 640 nm and of a positive Cotton effect at 385 nm was observed. After the addition of 1 equivalent of base, a plateau was reached at 620 nm, in agreement with the formation of the mononuclear $[Cu^{II}(H_2L^1)(OHCH_3)_n]^+$ complex. Further addition of base led to increasing negative Cotton effects at 716 and 565 nm and a further intensification of the band at 385 nm. A titration end-point at these wavelengths was observed after the addition of 3 equivalents of base, in agreement with the earlier results that indicated the formation of a dinuclear methoxide-bridged $[Cu^{II}_2(HL^1)(\mu\text{-}OCH_3)(OHCH_3)_n]^+$ complex.

EPR spectroscopy: X-band EPR spectroscopy was used to support the interpretation based on ESI-MS and UV/Vis spectroscopy. EPR spectra of solutions with different ratios of copper(II), H_3L^1, and base in methanol at 130 K exhibit axially symmetric copper(II) signals for the solvated copper(II) ion and a rhombically distorted signal for the mononuclear $[Cu^{II}(H_2L^1)(OHCH_3)_n]^+$ complex (see Supporting Information, Figure S1). The EPR signal intensity of $[Cu^{II}(H_2L^1)(OHCH_3)_n]^+$ is strongly dependent on the concentration of base, and this is consistent with the UV/Vis and ESI-MS studies. The most intense signal occurs at a 1:1:1 ratio of Cu^{II}/H_3L^1/base, and all signals vanish when an excess of base is added. The absence of any EPR signals for the dinuclear complex $[Cu^{II}_2(HL^1)(\mu\text{-}OCH_3)(OHCH_3)_n]^+$ is believed to be the result of strongly antiferromagnetically coupled copper(II) centers, induced by the bridging methanolate. This interpretation is supported by the room temperature magnetic moment of $\mu_{eff}=0.22$ BM of a solid sample and the corresponding EPR measurement (EPR silent; the presence of copper(II) in this sample is substantiated by UV/Vis, CD, and ESI-MS). Based on the satisfactory computer simulation of the experimental EPR spectrum of the mononuclear species (see Figure 4a,b), the existence of multiple mononuclear copper(II) complexes with different structures, for example involving the coordination of a copper(II) ion to the $N_{peptide}\text{-}N_{heterocycle}\text{-}N_{peptide}$ site, can be excluded.

EPR spectra of the mononuclear copper(II) complexes with $L=L^1$, L^2, and L^{wa} in methanol at 50 K reveal signals

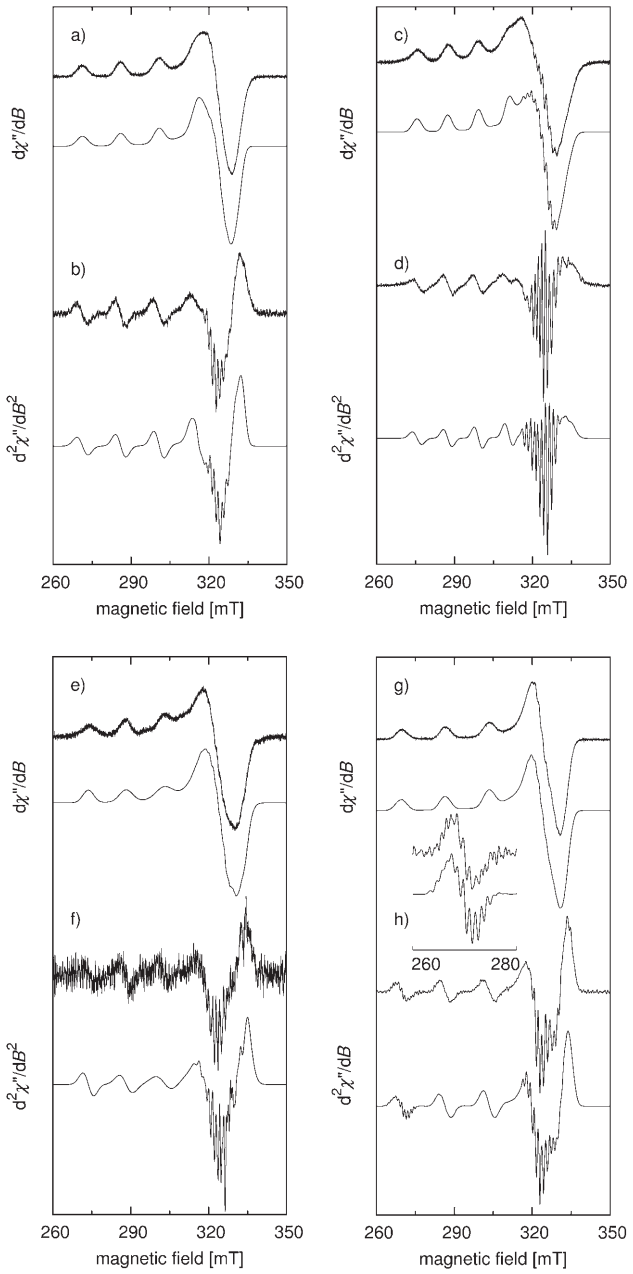

Figure 4. Experimental (top) and simulated (bottom) X-band EPR spectra of the mononuclear copper(II) complexes in methanol at 50 K: a) 1st derivative spectra of $[Cu^{II}(H_2L^1)(OHCH_3)_2]^+$, $\nu = 9.3571$ GHz; b) 2nd derivative spectra of a); c) 1st derivative spectra of $[Cu^{II}(H_2L^2)(OHCH_3)_2]^+$, $\nu = 9.3597$ GHz; d) 2nd derivative spectra of c); e) 1st derivative spectra of $[Cu^{II}(H_2L^3)(OHCH_3)_2]^+$, obtained from subtraction of experimental spectra with different L^3:Cu^{2+}:CH_3O^- ratios (see also Figure 5), $\nu = 9.3590$ GHz; f) 2nd derivative spectra of e); g) 1st derivative spectra of $[Cu^{II}(H_2L^{wa})(OHCH_3)_2]^+$, $\nu = 9.3588$ GHz; h) 2nd derivative spectra of g) (inset shows an expansion of the parallel $M_I = 3/2$ resonance).

of the pure mononuclear copper(II) complexes (Figure 4a,c,g). In contrast, EPR spectra of solutions of copper(II) triflate, H_3L^3, and base $[(n\mathrm{Bu}_4\mathrm{N})(OCH_3)]$ in various ratios (x:1:y; $x = 1,2$; $y = 1, 2, 3$) show resonances attributable to both mono- and dinuclear copper(II) complexes. Subtraction of spectra obtained at different ratios yields the pure spectra of the mono- and dinuclear copper(II) complexes shown in Figures 4e and 5.

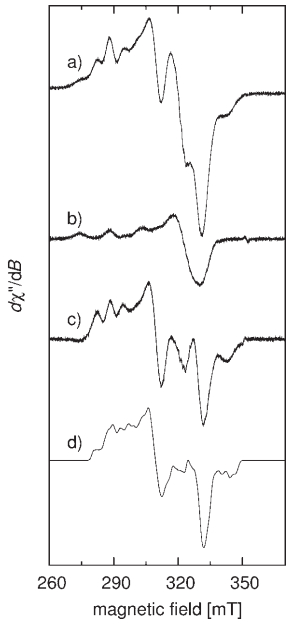

Figure 5. X-band EPR spectra of the copper(II) complexes of L^3 in methanol at 50 K: a) experimental spectrum (mixture of mono- and dinuclear complexes), $\nu = 9.3590$ GHz; b) $[Cu^{II}(H_3L^3)(OHCH_3)_2]^+$, obtained by subtracting experimental spectra with different concentrations of copper(II), ligand, and base; c) $[Cu^{II}_2(HL^3)(\mu\text{-}OCH_3)]^+$, obtained by subtracting b) from a); d) simulation of spectrum c).

Examination of the perpendicular region of the EPR spectra of the mononuclear complexes reveals nitrogen hyperfine coupling. Differentiation of the spectra and Fourier filtering produce well-resolved second-derivative EPR spectra with nitrogen hyperfine coupling in the perpendicular region, and for $[Cu(H_2L^{wa})(OHCH_3)_n]^+$ also on the parallel copper $M_I = 3/2$ hyperfine resonance (see Figure 4b,d,f,h). Computer simulations of the first- and second-derivative EPR spectra, based on the spin Hamiltonian of Equation (1),

$$H = \sum_{i=x,y,z} (\beta_e \underline{B}_i \cdot g_i \cdot \underline{S}_i + S_i \cdot A_i(^{63,65}\mathrm{Cu}) \cdot \underline{I}_i(^{63,65}\mathrm{Cu}) - g_n\beta_n \underline{B}_i \cdot \underline{I}_i(^{63,65}\mathrm{Cu})) + \sum_{j=1}^{3,4} (\underline{S}_i \cdot A_j(^{14,15}\mathrm{N}) \cdot \underline{I}_j(^{14,15}\mathrm{N}) - g_n\beta_n \underline{B}_i \cdot \underline{I}_j(^{14,15}\mathrm{N})) \quad (1)$$

and with the parameters listed in Table 1, yield the spectra shown in red in the Supporting Information; for line width parameters, Table S2. Least-squares error parameters of 0.02–0.04 for all simulations indicate excellent fits.[38] This is also apparent from expansions of the perpendicular region (see Supporting Information, Figure S2).

Table 1. Anisotropic spin Hamiltonian parameters of the mononuclear copper(II) species $[Cu^{II}(H_2L^1)(OCH_3)_2]^+$, $[Cu^{II}(H_2L^2)(OCH_3)_2]^+$, $[Cu^{II}(H_2L^3)(OCH_3)_2]^+$, and $[Cu^{II}(H_2L^{wa})(OCH_3)]^+$.[a]

	$[Cu^{II}(H_2L^1)(OCH_3)_2]^+$	$[Cu^{II}(H_2L^2)(OCH_3)_2]^+$	$[Cu^{II}(H_2L^3)(OCH_3)_2]^+$	$[Cu^{II}(H_2L^{wa})(OCH_3)]^+$
g_x	2.088	2.083	2.082	2.083
g_y	2.051	2.034	2.037	2.051
g_z	2.278	2.279	2.263	2.267
A_x (^{63}Cu)	17.0	17.3	15.7	14.0
A_y (^{63}Cu)	15.4	17.2	19.9	16.2
A_z (^{63}Cu)	153.4	123.0	150.0	175.0
A_x (^{14}N)–N_{hetcyc}[b]	14.5	15.7	14.3	12.4
A_y (^{14}N)–N_{hetcyc}[b]	7.1	7.1	7.0	6.2
A_z (^{14}N)–N_{hetcyc}[b]	9.0	9.0	9.0	10.4
A_x (^{14}N)–N_{pept} (+ N_{hetcyc})[c]	13.2	13.4	11.5	16.5
A_y (^{14}N)–N_{pept} (+ N_{hetcyc})[c]	15.2	14.1	15.7	12.7
A_z (^{14}N)–N_{pept} (+ N_{hetcyc})[c]	9.5	9.5	9.5	13.4

[a] A in 10^{-4} cm^{-1}; linewidth information is available as Supporting Information, Table S2. [b] Simulated spectra included two magnetically equivalent heterocyclic nitrogen nuclei. [c] For $[Cu^{II}(H_2L^{wa})]^+$.

EPR spectra of $[Cu(H_2L)(OCH_3)_n]^+$ (L = L^1, L^2, L^3; see Figure 4a–f) were simulated by assuming ligand hyperfine coupling to two magnetically equivalent heterocyclic nitrogen nuclei and one peptide nitrogen (see Table 1). In contrast, for the simulation of the EPR spectrum of $[Cu(H_2L^{wa})(OCH_3)_n]^+$, ligand hyperfine coupling to two magnetically equivalent heterocyclic nitrogen donors and two other nitrogen donors (one peptide and one heterocyclic nitrogen) had to be implemented in order to obtain a good fit (see Figure 4g,h; see also the Supporting Information, Figure S2).[39] The spin Hamiltonian parameters reveal a rhombically distorted square-pyramidal geometry for the copper(II) center in these cyclic peptide complexes. While the g matrices for the four copper(II) complexes are quite similar, A_z for $[Cu(H_2L^{wa})(OCH_3)_n]^+$ is considerably larger (174×10^{-4} cm^{-1} vs $\sim150\times10^{-4}$ cm^{-1}), which is consistent with the coordination of an additional nitrogen donor.[40] This interpretation is consistent with the analysis of the ligand hyperfine coupling (see above) and is supported by DFT modeling studies, see below.

The absence of signals for dinuclear copper(II) complexes results from strong antiferromagnetic coupling (H_3L^1, see above) and/or from low concentrations of the dicopper(II) complexes (H_3L^{wa}, H_3L^2), in agreement with the mass spectrometric data. The EPR spectra of solutions of copper(II) and H_3L^3 are indicative of mixtures of mono- and dinuclear copper(II) species (Figure 5a).

Careful subtraction yielded the spectra of the mono- and dinuclear copper(II) complexes, as shown in Figure 5b and c, respectively. The spin Hamiltonian parameters were obtained from a computer simulation (Figure 5d) with Molecular Sophe, based on the coupled spin Hamiltonian [Eq. (2)], which includes the individual spin Hamiltonians [Eq. (1)] for each copper(II) ion and isotropic and anisotropic exchange terms.[41]

$$H = \sum_{i,j=1;i\neq j}^{2} H_i + J_{ij}^{iso} S_i \cdot S_j + S_i \cdot J_{ij} \cdot S_j \qquad (2)$$

The spin Hamiltonian parameters for site 1 ($g_\parallel = 2.2090$, $g_\perp = 2.090$, $A_\parallel = 152.8$, $A_\perp = 5.2\times10^{-4}$ cm^{-1}, $\beta = -66.2°$, where β is the orientation of the g_z principal axis relative to the copper(II)···copper(II) vector) differ from those of site 2 ($g_\parallel = 2.209$, $g_\perp = 2.090$, $A_\parallel = 35.1$, $A_\perp = 21.4\times10^{-4}$ cm^{-1}, $\beta = -66.2°$), and the two sites are separated by an internuclear distance of $r = 5.0$ Å.[42] A Cu···Cu distance of 5 Å appears to be too large for the 18-membered azacrown-6 macrocyclic cavity (the more realistic computed distance is about 3.2 Å, see below). However, it is known that an anisotropic term proportional to $(\Delta g/g)^2 J$ can contribute to the zero-field splitting (S·J·S) if the isotropic exchange coupling constant is large ($J > 30$ cm^{-1}).[43] Therefore, with large values of J, which appears to be the case for the dinuclear copper(II) complex of H_3L^3, the simulation overestimates the internuclear distance r. Based on the DFT calculations (see below), site 2 has a distorted tetrahedral geometry with a coordinated thiazole, an amide nitrogen, and two relatively weakly bound ligands (two methanol/methanolate donors; one terminal, one bridging). Therefore, a small value of $A_\parallel$ is expected.[8,44–47]

IR spectroscopy: Upon coordination of H_3L^1 to copper(II), there is a shift of the $CO_{peptide}$ vibrational band in the IR spectrum from 1656 cm^{-1} in the metal-free macrocycle to 1617 cm^{-1} in the copper(II) complex. Such a shift would be expected for the substitution of hydrogen of a peptide group by a metal ion. The vibrations of the $N_{peptide}$–H bonds in the macrocycle H_3L^1 give rise to a sharp peak at 3378 cm^{-1}. A weaker, broad signal at 3292 cm^{-1} may be assigned to a single $N_{peptide}$–H bond in the dinuclear copper(II) complex of H_3L^1. That is to say, the complex has one protonated and two deprotonated amide sites and therefore a deprotonated bridging methanolate ligand, $[Cu^{II}_2(HL^1)(\mu\text{-}OCH_3)(OCH_3)_n]^+$ rather than $[Cu^{II}_2(L^1)(\mu\text{-}OHCH_3)(OCH_3)_n]^+$; see also the sections on mass spectrometry and DFT calculations. This assignment was confirmed by a comparison with the spectra of hydrogen–deuterium exchanged samples, obtained by preparing a solution of the compounds in CH_3OD. Figure 6 shows the IR spectra and frequencies of the

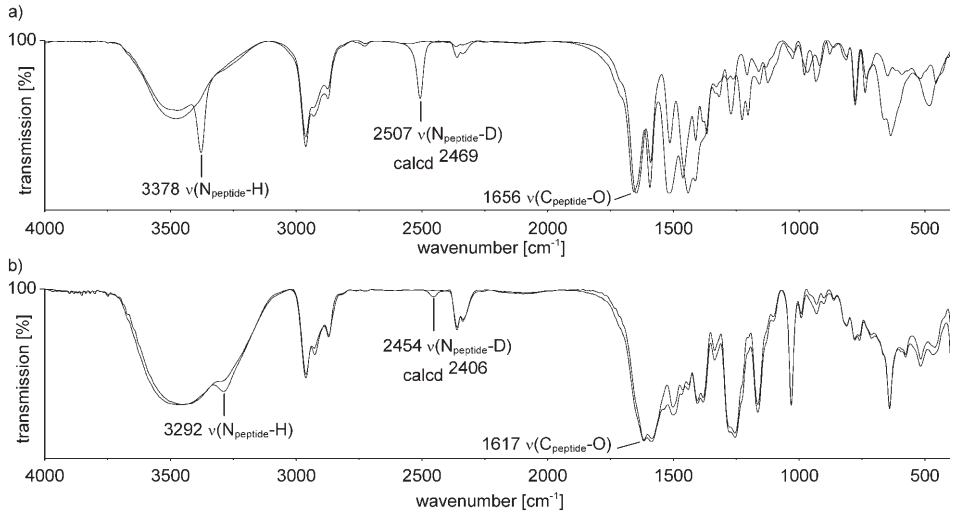

Figure 6. IR spectra (KBr pellets) of a) H_3L^1 and D_3L^1; b) $[Cu^{II}_2(HL^1)(\mu\text{-}OCH_3)](CF_3SO_3)$ and $[Cu^{II}_2(DL^1)(\mu\text{-}OCH_3)](CF_3SO_3)$.

$N_{peptide}$–H and $N_{peptide}$–D vibrations in the metal-free ligand H_3L^1 and the corresponding dinuclear copper(II) complex. An interesting observation is that $N_{peptide}$–H proton exchange in the dinuclear complex is very slow, even though the $N_{peptide}$–H bond is, as expected, weakened in the complex (3292 vs 3378 cm^{-1}). Complete exchange of the protons in the metal-free macrocycle H_3L^1 takes approximately 24 h, whereas proton exchange in the coordinated ligand requires approximately one week. This apparent anomaly may be explained in terms of an $N_{peptide}$–H···$O_{methoxide}$ hydrogen bond to the methoxide bridge, and this further supports the structural assignment.

Time-dependent spectroscopy: Subjecting solutions of the macrocyclic ligand H_3L^1 and copper(II) in methanol to time-dependent ESI mass spectrometry in conjunction with UV/Vis and EPR was indicative of an equilibrium involving only the mono- and dinuclear copper(II) complexes. The peak intensities of the protonated metal-free macrocycle $[H_4L^1]^+$ and the initially rapidly increasing peak of the mononuclear species $[Cu^{II}(H_2L^1)(OHCH_3)_n]^+$ decrease over time with respect to the increasing peak of the dinuclear species $[Cu^{II}_2(HL^1)(\mu\text{-}OCH_3)(OHCH_3)_n]^+$.

UV/Vis spectra of various mixtures of H_3L^1, copper(II) triflate, and $(n\text{Bu}_4\text{N})(OCH_3)$ in methanol initially show an overall increase of the absorption between 300 nm and 900 nm (Figure 7a,b). An equilibrium of only two competing copper(II) complexes is supported by the existence of isosbestic points at 354, 395, 490, and 605 nm. After approximately 30 min, the absorption intensifies below 354 nm, between 395 nm and 490 nm, and above 605 nm, while the absorption between 354 and 395 nm and between 409 and 605 nm decreases. The latter observation is attributed to the formation of the mononuclear $[Cu^{II}(H_2L^1)(OHCH_3)_n]^+$ complex, and the former to the copper(II) chromophore of the dinuclear complex $[Cu^{II}_2(HL^1)(\mu\text{-}OCH_3)(OHCH_3)_n]^+$ with a different coordination environment of the second copper(II) center. An equilibrium is reached after approximately 24 h, whereupon no further changes in the spectra are observed. These observations suggest that the fast formation of the mononuclear $[Cu^{II}(H_2L^1)(OHCH_3)_n]^+$ complex (within minutes under the given conditions) is followed by the much slower formation of the dinuclear complex $[Cu^{II}_2(HL^1)(\mu\text{-}OCH_3)(OHCH_3)_n]^+$.

Time-dependent X-band EPR spectra measured from frozen solutions in methanol at 130 K show a competition between free copper(II) and a single mononuclear species. Figure 7c shows the formation of a mononuclear copper(II) complex in a 1:1:1 mixture of H_3L^1, copper(II) triflate, and $(n\text{Bu}_4\text{N})(OCH_3)$ in methanol, identified as $[Cu^{II}(H_2L^1)(OHCH_3)_n]^+$. Note that, due to freezing of the sample, the time scale is arbitrary and different to that of the UV/Vis experiments described above. The absence of any further EPR signals, in particular for dinuclear copper(II) species, indicates strong antiferromagnetic coupling of the two copper(II) ions in the $[Cu^{II}_2(HL^1)(\mu\text{-}OCH_3)(OHCH_3)_n]^+$ complex (see above).

DFT calculations: The structures of the mono- and dinuclear copper(II) complexes were optimized starting from the predictions based on spectroscopic data (see Figure 8a–f, and Table 2). DFT calculations were performed with a setup previously optimized for copper(II) complexes.[48] Frequency calculations on the optimized structures were used to verify that they were indeed minima on the potential energy surface and to obtain zero-point energy corrections (ZPE). The mononuclear copper(II) complexes of H_3L ($L = L^1$, L^2, L^3) have a distorted square-pyramidal coordination geometry, with one peptide and two heterocyclic nitrogen atoms as well as a methanol oxygen donor in the basal plane and a methanol oxygen donor with a significantly longer bond in the apical position. A similar coordination geometry has been observed for copper(II) complexes of the larger Ascidiacyclamide macrocycle.[5] In agreement with the interpretation of the EPR spectra, structure optimization of the mononuclear copper(II) complex of H_3L^{wa} yielded a different coordination mode, with the copper(II) center coordinated to one peptide nitrogen and all three oxazoline nitrogen donors. In contrast to the macrocycles H_3L ($L = L^1$, L^2, L^3), the higher flexibility of H_3L^{wa} conferred by the unsaturated heterocyclic units leads to a conformation in which the third oxazoline nitrogen is able to coordinate

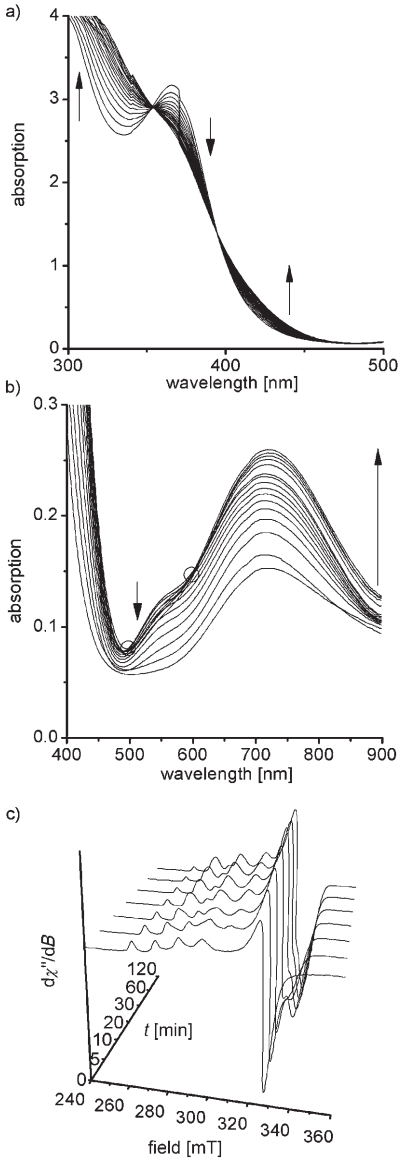

Figure 7. a) Time-dependent UV/Vis spectra of a 1:2:3 equiv mixture of L^1, copper(II) triflate, and base (methoxide); time interval between two spectra: 5 min; b) time-dependent UV/Vis spectra of a 1:1:1 equiv mixture of L^1, copper(II) triflate, and base (methoxide); time interval between two spectra: 5 min; c) time-dependent EPR spectra (X-band at 130 K) of a 1:1:1 equiv mixture of L^1, copper(II) triflate, and base (methoxide); $\nu_0 = 9.4483$ GHz, $\nu_5 = 9.4483$ GHz, $\nu_{10} = 9.4483$ GHz, $\nu_{20} = 9.4483$ GHz, $\nu_{30} = 9.4385$ GHz, $\nu_{60} = 9.4434$ GHz, $\nu_{120} = 9.4434$ GHz; time interval between two spectra (nonlinear scale): 0, 5, 10, 10, 30, 60 min.

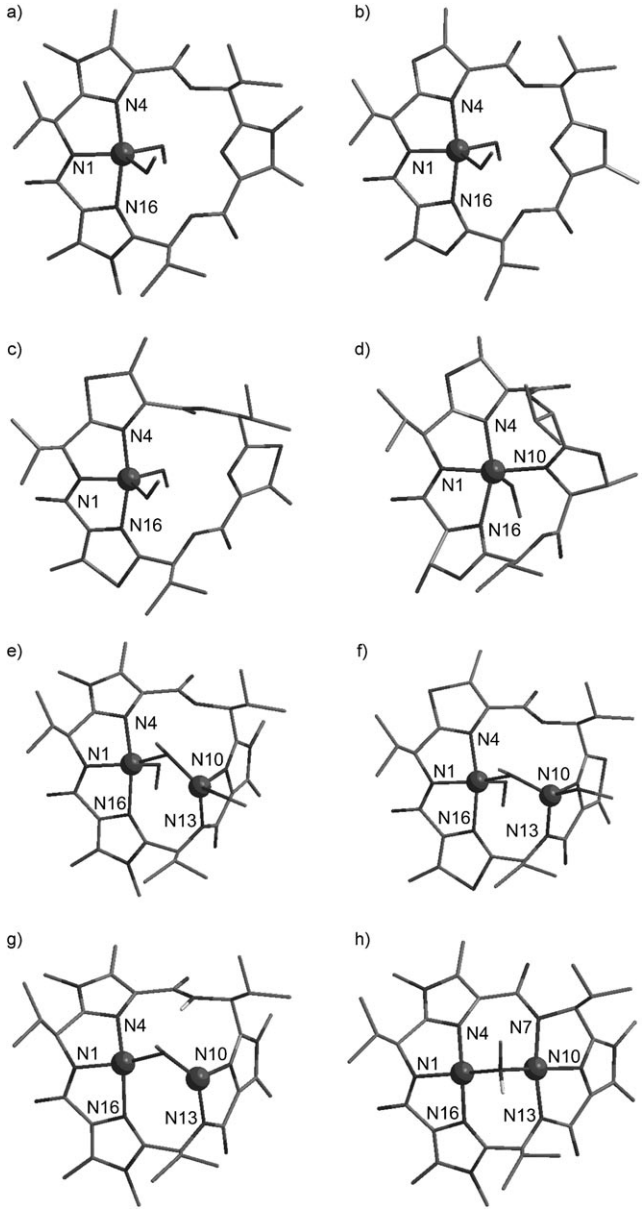

Figure 8. Calculated structures of the mononuclear copper(II) complexes: a) $[Cu^{II}(H_2L^1)]^+$; b) $[Cu^{II}(H_2L^2)]^+$; c) $[Cu^{II}(H_2L^3)]^+$; d) $[Cu^{II}(H_2L^{wa})]^+$, calculated structures of the dinuclear copper(II) complexes: e) $[Cu^{II}_2(HL^1)(\mu\text{-}OCH_3)]^+$; f) $[Cu^{II}_2(\mu\text{-}HOCH_3)(L^1)(OHCH_3)]^+$; g) $[Cu^{II}_2(HL^1)(\mu\text{-}OCH_3)]^+$; h) $[Cu^{II}_2(\mu\text{-}HOCH_3)(L^3)]^+$.

to the copper(II) center. One methanol molecule coordinated to the axial site completes the coordination sphere.

The structures of dinuclear copper(II) complexes with H_3L^1 and H_3L^3 were also refined, and the two complexes predicted by spectroscopy, that is, $[Cu^{II}_2(HL^1)(\mu\text{-}OCH_3)(OHCH_3)_n]^+$ and $[Cu^{II}_2(HL^3)(\mu\text{-}OCH_3)(OHCH_3)_n]^+$, were indeed found to be stable minima on the potential energy surface. As indicated by IR spectroscopy, the structure with a μ-OCH_3 bridge and only two deprotonated amide groups is more stable than the tautomer with three deprotonated amides and a bridging methanol. Two additional methanol molecules were added as co-ligands. The second copper(II) center has a distorted tetrahedral coordination geometry (Figure 8g,h and Table 2), and this is in agreement with the simulation and interpretation of the EPR spectra of the copper(II) complexes of H_3L^3. The strength of the antiferromagnetic coupling in OR-bridged dicopper(II) complexes depends on the Cu^{II}-O-Cu^{II} angle.[49–51] The computed structures of $[Cu^{II}_2(HL)(\mu\text{-}OCH_3)(OHCH_3)_2]^+$ ($L = L^1$, L^3) are in agreement with these dependences and with the observation that the complex of the imidazole-based ligand shows stronger coupling than the complex of the thiazole-based ligand,

Table 2. Selected computed (B3LYP) structural parameters (distances [Å] and angles [°]) of the mono- (1–4; $[Cu^{II}(H_2L)(OHCH_3)_n]^+$; L = L^1, L^2, L^3, L^{wa}) and dinuclear complexes (5, 6; $[Cu^{II}_2(H_mL)(\mu\text{-}H_nOCH_3)(OHCH_3)_2]^+$; L = L^1, L^2, L^3, L^{wa}; $n = 0, 1$; $m = 0, 1$; see Figure 8).

			Distances [Å]				
Structure	Cu1–N1	Cu1–N4,N16,N10	Cu1–X_1,X_2[a]	Cu2–N10	Cu2–N13	Cu2–X_3,X_4[b]	Cu1···Cu2
a)	1.91	2.03, 2.05, –	2.07, 2.39	–	–	–	–
b)	1.92	2.02, 2.03, –	2.00, 2.43	–	–	–	–
c)	1.92	2.01, 2.01, –	2.04, 2.37	–	–	–	–
d)	1.94	2.05, 2.10, 2.11	2.11, 2.36	–	–	–	–
e)	1.90	2.06, 2.10, –	2.00, 2.65	1.95	1.89	1.90, 2.12	3.08
f)	1.88	2.12, 2.07, –	1.99, 2.48	1.93	1.88	1.89, 2.17	3.20
			Angles [°]				
Structure	N1-Cu1-N4,N16	N1-Cu1-X_1,X_2	X_1-Cu1-X_2	N10-Cu2-N13	N10-Cu2-X_3	N10-Cu2-X_4	Cu1-X-Cu2
a)	83.3, 83.1	143.8, 108.2	107.8	–	–	–	–
b)	83.6, 83.8	144.8, 106.8	108.3	–	–	–	–
c)	82.4, 82.9	135.1, 104.2	120.6	–	–	–	–
d)	79.3, 80.1	158.1, 109.8	92.0	–	–	–	–
e)	82.8, 83.7	147.0, 106.9	104.9	86.0	105.9	126.1	104.7
f)	82.1, 83.1	143.1, 111.3	105.1	85.7	125.9	107.2	111.6

[a] X_1: in plane; X_2: axial. [b] X_3: μ-OCH_3; X_4: $OHCH_3$.

for which a dipole–dipole-coupled spectrum is observed (see Figure 5).

The two possible isomers of the dinuclear L^1-based complexes with respect to the bridging methanol/amide tautomerism, $[Cu^{II}_2(HL^1)(\mu\text{-}OCH_3)]^+$ (Figure 8g) and $[Cu^{II}_2(\mu\text{-}HOCH_3)(L^1)]^+$ (Figure 8h), both without additional methanol ligands, were also optimized in order to compare their relative stabilities. As suggested by experiment, the structure with a bridging methanolate and a protonated and not coordinated amide is more stable by a large margin (129 kJ mol^{-1}).

Conclusion

Westiellamide (H_3L^{wa}) and the three analogues H_3L^1, H_3L^2, and H_3L^3 are highly preorganized for binding to metal ions and are complementary for copper(II). As in the larger cyclic peptides ascidiacyclamide and patellamide, the $N_{heterocycle}$-$N_{peptide}$-$N_{heterocycle}$ unit is the preferred coordination site for copper(II).[5,6] Westiellamide and its derivatives form stable mono- and dinuclear complexes. Particularly with H_3L^1, there is a cooperativity in the formation of the dinuclear species, that is, the coordination of a first copper(II) ion further preorganizes the macrocycle, and this is enhanced by the coordination of monodentate methanol (or water), which may play an anchoring role and stabilize the dinuclear complexes as a bridging ligand. With the more flexible oxazoline donors, westiellamide H_3L^{wa} forms more stable mononuclear complexes, with four instead of three heterocyclic units and an amide moiety coordinated in-plane, and only one methanol in the apical position. Coordination of a second copper(II) center is therefore less favorable for this peptide.

Experimental Section

Materials: All solvents (absolute) and reagents (purum grade) were obtained commercially (Aldrich, Fluka) and were used without further purification. Westiellamide (H_3L^{wa}) and macrocycles H_3L^1, H_3L^2, and H_3L^3 were prepared according to published procedures.[34,52]

Solid samples of $[Cu^{II}_2(HL^1)(\mu\text{-}OCH_3)](CF_3SO_3)$ and $[Cu^{II}_2(DL^1)(\mu\text{-}OCH_3)](CF_3SO_3)$ (green powders) were obtained by mixing $Cu(CF_3SO_3)_2$, $Cu(OMe)_2$, and H_3L^1 or D_3L^1 (0.5:1.5:1) in dry methanol (CH_3OH or CH_3OD, respectively). The resulting samples were characterized by ESI-MS and UV/Vis spectrophotometry (both in methanol) and shown to be identical to the corresponding samples from titration experiments. An elemental analysis (calcd (%) for $C_{32}H_{46}Cu_2F_3N_9O_7S\cdot 2H_2O$: C 41.73, H 5.47, N 13.69; found: C 40.39, H 5.47, N 13.63) confirmed this assignment and indicated a purity of >95%. Further purification was not possible. The room temperature magnetic moments and EPR spectra (in methanol) showed these samples to be diamagnetic (strong antiferromagnetic coupling). These samples were used for IR spectroscopy.

Methods: High-resolution electrospray ionization mass spectrometry (ESI-MS) was performed with a 9.4 T Bruker ApexQe Qh-ICR hybrid instrument with an Apollo II MTP ion source in the positive-ion electrospray ionization (ESI) mode. Sample solutions in methanol or acetonitrile at concentrations of 10^{-4}–10^{-5} M were admitted to the ESI interface by means of a syringe pump at 5 μL min^{-1} and sprayed at 4.5 kV with a desolvation gas flow of 2.0 L min^{-1} at 250 °C and a nebulizer gas flow of 1.0 L min^{-1}. The ions were accumulated in the storage hexapole for 0.1–1.0 s and then transferred into the ICR cell. Trapping was achieved at a sidekick potential of −4.0 V and trapping potentials of slightly above 1 V. The mass spectra were acquired in the broadband mode with 1 M data points. Typically, 16 transients were accumulated for one magnitude spectrum. External mass calibration was performed on $[arginine_n+H]^+$ cluster ions prior to analysis. A mass accuracy of 1 ppm was achieved. The instrument was controlled by Bruker ApexControl 2.0.0.beta software and data analysis was performed using Bruker DataAnalysis 3.4 software.

Spectrophotometric titrations were performed at 25.0 °C on 20 cm^3 samples at a ligand concentration of 2.0×10^{-3} mol dm^{-3} with a ligand/copper(II) ratio of 1:1 in acetonitrile and 1:2 in methanol. The titrations were performed with a 665 Dosimat automatic buret (Metrohm) containing either a solution of tetrabutylammonium methoxide in methanol or a solution of triethylamine in acetonitrile (~0.02 M). The absorbance data were recorded with a TIDAS II (J&M) spectrophotometer, equipped with a Hellma 661.202 UVS external immersion probe (pathlength 1 cm). For each measurement, 51 titration points were recorded.

IR spectra were measured with a Perkin Elmer 16C FTIR instrument from samples in KBr pellets.

UV/Vis/NIR spectra were recorded in methanol ($\mu = 0.1$ M (nBu$_4$N)(ClO$_4$), $c(H_3L^1) = 1.5$ mM, pathlength $l = 1$ cm) at 25.0 °C with a JASCO V-570 spectrophotometer.

CD spectra were measured in methanol ($\mu = 0.1$ M (nBu$_4$N)(ClO$_4$), $c(H_3L^1) = 1.25$ mM, pathlength $l = 1$ cm) at 25 °C with a JASCO J-710 spectropolarimeter.

Magnetic moments were measured with a Sherwood Scientific Mark 1 magnetic susceptibility balance at room temperature.

Continuous-wave X-band (ca. 9 GHz) EPR spectra were recorded with a Bruker Biospin Elexsys E500 EPR spectrometer fitted with a super high Q cavity. The magnetic field and the microwave frequency were calibrated with a Bruker ER 041XK Teslameter and a Bruker microwave frequency counter, respectively. A flow-through cryostat in conjunction with a Eurotherm (B-VT-2000) variable-temperature controller provided temperatures of 127–133 K at the sample position in the cavity. For lower temperatures (48–52 K), an Oxford Instruments ESR 900 flow-through cryostat in conjunction with an ITC4 temperature controller was employed. Spectrometer tuning, signal averaging, and visualization were accomplished with Bruker's Xepr (version 2.4b.12) software. The EPR spectra of the mono- and dinuclear complexes were simulated with the XSophe-Sophe-XperView (version 1.1.4) and Molecular Sophe (version 2.0.91) computer simulation software suites on a personal computer running the Mandriva Linux v2007.0 operating system.[38]

DFT calculations were performed with Gaussian 03 using the hybrid B3LYP functional and the 6-31g* basis set and were run on a Linux cluster.[53]

Acknowledgements

Generous financial support from the German Science Foundation (DFG) is gratefully acknowledged. We thank Dr. J. H. Gross (Mass spectrometry facility, Institute of Organic Chemistry, University of Heidelberg) for measuring the ESI mass spectra and for assistance with their interpretation.

[1] P. Wipf, S. Venkatraman, C. P. Miller, S. J. Geib, *Angew. Chem.* **1994**, *106*, 1554–1556; *Angew. Chem. Int. Ed. Engl.* **1994**, *33*, 1516–1518.
[2] C. J. Hawkins, *Pure Appl. Chem.* **1988**, *60*, 1267–1270.
[3] B. M. Degnan, C. J. Hawkins, M. F. Lavin, E. J. McCaffrey, D. L. Parry, A. L. van den Brenk, D. J. Watters, *J. Med. Chem.* **1989**, *32*, 1349–1354.
[4] J. P. Michael, G. Pattenden, *Angew. Chem.* **1993**, *105*, 1–24; *Angew. Chem. Int. Ed. Engl.* **1993**, *32*, 1–23.
[5] A. L. van den Brenk, K. A. Byriel, D. P. Fairlie, L. R. Gahan, G. R. Hanson, C. J. Hawkins, A. Jones, C. H. L. Kennard, B. Moubaraki, K. S. Murray, *Inorg. Chem.* **1994**, *33*, 3549–3557.
[6] A. L. van den Brenk, D. P. Fairlie, G. R. Hanson, L. R. Gahan, C. J. Hawkins, A. Jones, *Inorg. Chem.* **1994**, *33*, 2280–2289.
[7] A. L. van den Brenk, D. P. Fairlie, L. R. Gahan, G. R. Hanson, T. W. Hambley, *Inorg. Chem.* **1996**, *35*, 1095–1100.
[8] P. Comba, R. Cusack, D. P. Fairlie, L. R. Gahan, G. R. Hanson, U. Kazmaier, A. Ramlow, *Inorg. Chem.* **1998**, *37*, 6721–6727.
[9] D. J. Freeman, G. Pattenden, A. F. Drake, G. Siligardi, *J. Chem. Soc. Perkin Trans. 2* **1998**, 129–136.
[10] L. Grondahl, N. Sokolenko, G. Abbenante, D. P. Fairlie, G. R. Hanson, L. R. Gahan, *J. Chem. Soc. Dalton Trans.* **1999**, 1227–1234.
[11] R. M. Cusack, L. Grondahl, G. Abbenante, D. P. Fairlie, L. R. Gahan, G. R. Hanson, T. W. Hambley, *J. Chem. Soc. Perkin Trans. 2* **2000**, 323–331.
[12] L. A. Morris, M. Jaspars, *Spec. Publ. R. Soc. Chem.* **2000**, *257*, 140–166.
[13] A. J. Blake, J. S. Hannam, K. A. Jolliffe, G. Pattenden, *Synlett* **2000**, 1515–1518.
[14] L. A. Morris, M. Jaspars, J. J. Kettenes-van den Bosch, K. Versluis, A. J. R. Heck, S. M. Kelly, N. C. Price, *Tetrahedron* **2001**, *57*, 3185–3197.
[15] L. A. Morris, B. F. Milne, M. Jaspars, J. J. Kettenes-van den Bosch, K. Versluis, A. J. R. Heck, S. M. Kelly, N. C. Price, *Tetrahedron* **2001**, *57*, 3199–3207.
[16] P. V. Bernhardt, P. Comba, D. P. Fairlie, L. R. Gahan, G. R. Hanson, L. Lotzbeyer, *Chem. Eur. J.* **2002**, *8*, 1527–1536.
[17] R. M. Cusack, L. Grondahl, D. P. Fairlie, L. R. Gahan, G. R. Hanson, *J. Chem. Soc. Perkin Trans. 2* **2002**, 556–563.
[18] L. A. Morris, B. F. Milne, G. S. Thompson, M. Jaspars, *J. Chem. Soc. Perkin Trans. 2* **2002**, 1072–1075.
[19] A. L. van den Brenk, J. D. A. Tyndall, R. M. Cusack, A. Jones, D. P. Fairlie, L. R. Gahan, G. R. Hanson, *J. Inorg. Biochem.* **2004**, *98*, 1857–1866.
[20] M. P. Foster, G. P. Concepción, G. B. Caraan, C. M. Ireland, *J. Org. Chem.* **1992**, *57*, 6671–6675.
[21] A. K. Todorova, F. Juettner, A. Linden, T. Pluess, W. von Philipsborn, *J. Org. Chem.* **1995**, *60*, 7891–7895.
[22] Y.-M. Li, J. C. Milne, L. L. Madison, R. Kolter, C. T. Walsh, *Science* **1996**, *274*, 1188–1193.
[23] P. Wipf, P. C. Fritch, S. J. Geib, A. M. Sefler, *J. Am. Chem. Soc.* **1998**, *120*, 4105–4112.
[24] R. S. Roy, A. M. Gehring, J. C. Milne, P. J. Belshaw, C. T. Walsh, *Nat. Prod. Rep.* **1999**, *16*, 249–263.
[25] H. C. Krebs, *Progress in the Chemistry of Organic Natural Products*, Springer, Vienna, **1986**, pp. 151–363.
[26] D. P. Fairlie, G. Abbenante, D. R. March, *Curr. Med. Chem.* **1995**, *2*, 654–686.
[27] C. W. Holzapfel, W. J. v. Zyl, *Tetrahedron* **1990**, *46*, 649–660.
[28] J. Ogino, R. E. Moore, G. M. L. Patterson, C. D. Smith, *J. Nat. Prod.* **1996**, *59*, 581–586.
[29] A. L. van den Brenk, G. R. Hanson, C. J. Hawkins, *J. Inorg. Biochem.* **1989**, *98*, 165.
[30] M. R. Prinsep, R. E. Moore, I. A. Levine, G. M. L. Patterson, *J. Nat. Prod.* **1992**, *55*, 140–142.
[31] P. Wipf, C. P. Miller, *J. Am. Chem. Soc.* **1992**, *114*, 10975–10977.
[32] T. W. Hambley, C. J. Hawkins, M. F. Lavin, A. van den Brenk, D. J. Watters, *Tetrahedron* **1992**, *48*, 341–348.
[33] G. Haberhauer, F. Rominger, *Tetrahedron Lett.* **2002**, *43*, 6335–6338.
[34] G. Haberhauer, F. Rominger, *Eur. J. Org. Chem.* **2003**, 3209–3218.
[35] G. Haberhauer, A. Pinter, T. Oeser, F. Rominger, *Eur. J. Org. Chem.* **2007**, 1779–1792.
[36] P. Wipf, C. Wang, *Org. Lett.* **2006**, *8*, 2381–2384.
[37] H. Sigel, R. B. Martin, *Chem. Rev.* **1982**, *82*, 385–426.
[38] G. R. Hanson, K. E. Gates, C. J. Noble, M. Griffin, A. Mitchell, S. Benson, *J. Inorg. Biochem.* **2004**, *98*, 903–916.
[39] Spectral resolution did not allow the determination of individual nitrogen hyperfine matrices for the peptide and heterocyclic nitrogen donors.
[40] J. Peisach, W. E. Blumberg, *Arch. Biochem. Biophys.* **1974**, *165*, 691–708.
[41] G. R. Hanson, C. J. Noble, S. Benson, *Biol. Magn. Reson.* **2007**, *28*, in press.
[42] Note that the quality of the experimental spectra (deconvoluted from that of a mixture of mono- and dinuclear species) and the corresponding simulation does not allow an accurate determination of all parameters. Therefore, the g values and β for the two sites are presumably not identical, and $A_\parallel$ of site 2 is very small but not necessarily as small as 35.1×10^{-4} cm^{-1}.
[43] T. D. Smith, J. R. Pilbrow, *Coord. Chem. Rev.* **1974**, 173–278.
[44] The $A_\parallel$ values for copper(II) complexes with four imidazole-derived donors in tetrahedral and square-planar arrangements are 118×10^{-4} and 178×10^{-4} cm^{-1}, respectively.
[45] S. Knapp, T. P. Keenan, X. Zhang, R. Fikar, J. A. Potenza, H. J. Schugar, *J. Am. Chem. Soc.* **1990**, *112*, 3452–3464.
[46] $A_\parallel$ of a copper(II) tetraamine complex with a square-planar arrangement of the amine donors is around 200×10^{-4} cm^{-1}, as compared to 119×10^{-4} cm^{-1} for copper(II) in MeOH.

[47] P. Comba, T. W. Hambley, M. A. Hitchman, H. Stratemeier, *Inorg. Chem.* **1995**, *34*, 3903–3911.
[48] M. Atanasov, P. Comba, B. Martin, V. Mueller, G. Rajaraman, H. Rohwer, S. Wunderlich, *J. Comput. Chem.* **2006**, *27*, 1263–1277.
[49] D. J. Hodgson, *Prog. Inorg. Chem.* **1975**, *19*, 173–241.
[50] M. Atanasov, C. Daul, *Chimia* **2005**, *59*, 504–510.
[51] M. Atanasov, C. A. Daul, *Chem. Phys. Lett.* **2003**, *379*, 209–215.
[52] P. Wipf, C. P. Miller, C. M. Grant, *Tetrahedron* **2000**, *56*, 9143–9150.
[53] Gaussian 03, Revision C.01, M. J. Frisch, G. W. Trucks, H. B. Schlegel, G. E. Scuseria, M. A. Robb, J. R. Cheeseman, J. A. Montgomery, T. Vreven Jr., K. N. Kudin, J. C. Burant, J. M. Millam, S. S. Iyengar, J. Tomasi, V. Barone, B. Mennucci, M. Cossi, G. Scalmani, N. Rega, G. A. Petersson, H. Nakatsuji, M. Hada, M. Ehara, K. Toyota, R. Fukuda, J. Hasegawa, M. Ishida, T. Nakajima, Y. Honda, O. Kitao, H. Nakai, M. Klene, X. Li, J. E. Knox, H. P. Hratchian, J. B. Cross, C. Adamo, J. Jaramillo, R. Gomperts, R. E. Stratmann, O. Yazyev, A. J. Austin, R. Cammi, C. Pomelli, J. W. Ochterski, P. Y. Ayala, K. Morokuma, G. A. Voth, P. Salvador, J. J. Dannenberg, V. G. Zakrzewski, S. Dapprich, A. D. Daniels, M. C. Strain, O. Farkas, D. K. Malick, A. D. Rabuck, K. Raghavachari, J. B. Foresman, J. V. Ortiz, Q. Cui, A. G. Baboul, S. Clifford, J. Cioslowski, B. B. Stefanov, G. Liu, A. Liashenko, P. Piskorz, I. Komaromi, R. L. Martin, D. J. Fox, T. Keith, M. A. Al-Laham, C. Y. Peng, A. Nanayakkara, M. Challacombe, P. M. W. Gill, B. Johnson, W. Chen, M. W. Wong, C. Gonzalez, J. A. Pople, Gaussian Inc., Wallingford CT, **2004**.

Received: November 12, 2007
Published online: March 28, 2008

